

# Conceptional design of nano-particulate ITO inks for inkjet printing of electron devices

Nadja Kölpin · Moritz Wegener · Erik Teuber ·  
Sebastian Polster · Lothar Frey · Andreas Roosen

Received: 18 June 2012 / Accepted: 22 September 2012 / Published online: 6 October 2012  
© Springer Science+Business Media New York 2012

**Abstract** This manuscript presents the conceptional design of indium tin oxide inkjet inks for the manufacture of electron devices. For this purpose, the process window of the printer used is identified and the inks are conceived to meet the requirements. The nano-particles are effectively stabilized in different dispersion media. The rheological, the wetting and the drying behavior of the inks are adapted to the inkjet process and the substrates to be coated. To assemble a field effect transistor (FET), the most suitable ink is chosen and source and drain contacts are printed. In the device, a nano-particulate ZnO layer acts as semiconducting layer and the gate electrode as well as the dielectric layer is formed by a thermally oxidized silicon wafer. The electron device assembled shows the typical FET characteristic proving its functionality.

## Introduction

Inkjet printing is an emerging technology with many potential applications in the field of electronics and

biotechnology such as the assembly of organic electron devices, the direct printing of electronic bonds on circuits or the manufacture of “gene chips” [1–3]. Compared to more conventional printing methods like screen printing or offset printing, inkjet printing is more flexible as it is a direct printing technique and it is also contactless, which can be advantageous for sensitive substrates.

The inkjet printing technique was initially developed in the 1960s and 1970s using a continuous jet for industrial applications. Later on in the 1970s and 1980s the drop-on-demand printers using piezo or bubble jet technology were developed [4]; the printers with piezo heads are still very frequently used for research activities today because they can be applied to a broad variety of inks [5–8].

Fromm [9] made a contribution to the understanding of the printability of the inks by numerically calculating the fluid dynamics of drop-on-demand jets using Navier–Stokes equations. In order to describe the fluid properties, he used the Reynolds  $N_{Re}$  number and the Weber number  $N_{We}$  of the ink:

$$N_{Re} = \frac{va\rho}{\eta} \quad (1)$$

$$N_{We} = \frac{v^2a\rho}{\sigma} \quad (2)$$

where  $v$  is the velocity,  $a$  is a characteristic dimension, i.e., the radius of the printing orifice, and  $\rho$ ,  $\eta$ , and  $\gamma$  are the fluid density, viscosity and surface tension, respectively. These two parameters can be summarized to the so-called parameter  $Z$ , which is the inverse of the Ohnesorge number  $Oh$  [10, 11].

$$Z = Oh^{-1} = \frac{N_{Re}}{\sqrt{N_{We}}} = \frac{\sqrt{a \cdot \rho \cdot \gamma}}{\eta} \quad (3)$$

For inkjet inks, the  $Z$ -parameter should lie in between 1 and 14 [10, 11]. If the ink fulfills this condition, then a drop

---

N. Kölpin · M. Wegener · A. Roosen (✉)  
Department of Materials Science, Glass and Ceramics,  
University of Erlangen-Nuremberg, Erlangen, Germany  
e-mail: andreas.roosen@ww.uni-erlangen.de

M. Wegener  
e-mail: moritz.wegener@ww.uni-erlangen.de

E. Teuber  
Fraunhofer Institute for Integrated Systems and Device  
Technology, Erlangen, Germany

S. Polster · L. Frey  
Department of Electrical, Electronic and Communication  
Engineering, University of Erlangen-Nuremberg, Erlangen,  
Germany

can be ejected out of the nozzle. For smaller  $Z$  values, the viscosity is the dominant parameter and the pressure pulse for ejection is dissipated by the fluid. If the  $Z$  value is too high, a comparably high liquid column is ejected out of the nozzle and satellite drops form instead of one single drop. Considering the formula above, it is clearly visible that for the creation of particle based inks the requirement to keep low viscosities at high particle contents is challenging [10].

Furthermore, beside the  $Z$ -parameter also the impact of the ink on the substrate and their interaction as well as the subsequent solidifying process have to be considered in order to achieve good print results [12]. Several publications have shown that the stability of printed lines is influenced by the wetting behavior of the ink on the substrate, the drying behavior of the ink, and processing parameters like the printing speed and the drop spacing [13–15]. The interaction of these parameters is complex, but as a general rule stable lines are preferentially formed if the contact angle of the ink on the substrate is low and the printing speed is high. Furthermore, the drop spacing has to be high enough to avoid bulging, but small enough to avoid the printing of single drops [15].

## Experiments

### Preparation of dispersions and inks

For the preparation of inks, nano-particles from Evonik Industries AG, Germany were applied (VP ITO TC 8). The powder exhibited a specific surface area of  $47.6 \text{ m}^2/\text{g}$ , which was determined by BET (ASAP 2000, Micromeritics Instrument Corp., Norcross, GA, USA). This corresponds to a diameter of 19 nm. This is confirmed by TEM micrographs (Philips CM 30, Eindhoven, NL) of the indium tin oxide (ITO) particles which indicate primary particles with a diameter of 15–20 nm, but which form agglomerates (Fig. 1). As reported earlier [16, 17], the ITO particles can be effectively stabilized in organic solvents using 3,6,9-trioxadecanoic acid (TODA, Sigma Aldrich, Milwaukee, WI, USA). By dynamic light scattering agglomerate sizes of approximated 100 nm were determined by using TODA as stabilizer. TODA acts mainly as a steric stabilizer, which was shown by Mahajeri et al. [18] using a laser Doppler electrophores method. By helium pycnometry (ScuPyc 1330, Micromeritics, USA) the density of the powder was determined to be  $6.51 \pm 0.01 \text{ g}/\text{cm}^3$ . ICP analysis (Spectro Analytical Instruments GmbH, Kleve, D) gave the result that the used ITO powder consist of 95.25 mass% In and 4.75 mass% Sn.

To study the dispersibility of the particles in different solvents, dispersions with solids contents of 2.7 to 14.4 vol. % ITO were prepared in ethanol, ethylene glycol,

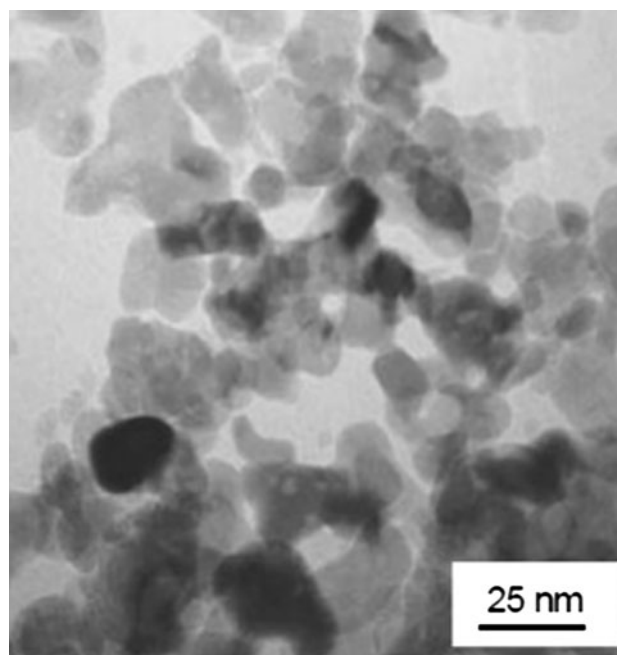


**Fig. 1** TEM micrograph of the ITO powder (particles and agglomerates)

**Table 1** Composition of ITO inks

	Composition of ink (vol.%)			Solvent composition (vol.%)		
	ITO	TODA	Solvent	Water	Ethanol	Ethylene glycol
Ink 1_6.9	6.9	1.3	91.8	29.9	25.2	44.9
Ink 2_2	2.0	0.4	97.6	15.5	19.6	65.0
Ink 2_6.9	6.9	1.3	91.8	15.5	19.6	65.0
Ink 2_9	9.0	1.7	89.3	15.5	19.6	65.0
Ink 3_6.9	6.9	1.3	91.8	5.0	31.7	63.2

and water. A dispersant content of 19 vol. % TODA with respect to the ITO content was applied. For the preparation of inks, ITO particles were always dispersed in a mixture of the three solvents according to the compositions given in Table 1. In order to study the influence of the types of solvents on the printing behavior of the inks and the geometry of the printed structures, three different solvent mixtures 1–3 are used. In order to examine the influence of the solids loading in the inks on the print result, three different solids loadings 2, 6.9, and 9 vol. % were used in combination with solvent mixture 2. Inks are denominated according to the solvent mixture (first number) and the solids loading in the dispersion (second number).

The dispersion preparation was done in a tumbling mixer (Turbula, Willy A. Bachofen AG, Basel, Swiss) with yttria stabilized zirconia milling balls of 0.1, 1.3, 2.3, and

10 mm in diameter for 24 h. Afterwards, the milling balls were separated from the dispersions using steel screens. As the increased viscosities of dispersions with higher solids loadings make the separation of small milling balls very difficult, no milling balls with diameters 0.1 mm were applied in dispersions of pure solvents above solids contents of 6.9 vol. %. Inks for inkjet printing were always prepared with milling balls with diameters of 0.1 mm because a minimum agglomerate size must be achieved in these dispersions to prevent the clogging of the nozzle during printing.

#### Characterization of dispersions and inks

The remaining agglomerate size in dispersions as well as in inks was determined using dynamic light scattering measurements (DLS; Ultra Fine Particle Analyzer UPA150, Microtrac, North Largo, FL). The rheological behavior of the dispersions and the inks was characterized using a rheometer in cone/plate arrangement with a cone diameter  $d_{\text{cone}}$  of 50 mm at a temperature of 20 °C (Physica UDS 200, PaarPhysica, Stuttgart, Germany). Rotational measurements were conducted with shear rates up to 200 s<sup>-1</sup>. To gain deeper insight in the structure of the dispersions and inks, also oscillatory measurements were performed. An angular frequency of 10 s<sup>-1</sup> was applied and the deformation was increased logarithmically up to 10,000 %. The surface tension and the wetting behavior of the dispersions and inks were studied using pendant drop and sessile drop measurements (Contact Angle System OCA 30, Dataphysics Instruments, Filderstadt, Germany). The surface tension was determined for dispersions with varied solids loadings using dosage needles with a diameter of 1.8 mm (GLT Löttechnik, Pforzheim, Germany). For the inks prepared, surface tensions as well as contact angle measurements were conducted. Contact angles were determined on silicon wafers and PET films, which were also used as substrates for inkjet printing. For sessile drop measurements, several small drops of dispersion were applied manually with syringes. For all dispersions and inks, the surface tensions and the contact angles, respectively, were averaged over three to seven measurements. Furthermore, the surface tensions of the PET and wafer substrates were determined using water, diiodomethane, and formamide.

#### Printing of the inks

Selected inks were printed with a commercial inkjet printer, which uses a piezo drop-on-demand-technique (Dimatix Materials Printer DMP-2800 Series, FUJIFILM Dimatix Inc., Santa Clara, CA, USA). Cartridges of type DMC-11610 with a nozzle diameter of 21.5 μm were used.

One to two nozzles were used for printing. An acceleration voltage in the range of 15–40 V was adapted to the printed inks individually in such a way, that only one drop per pulse was ejected and no satellite drops were generated. This was controlled using the drop-watch function of the device. To compare the print results, a test pattern of horizontal lines was printed with single drops with spaces in the range of 20–120 μm.

#### Characterization of printed structures

The printed structures were characterized concerning their dimensions and their microstructure using microscopy: SEM micrographs were taken of the drops on the wafer (Quanta 200, FEI, Eindhoven, The Netherlands). The topography of the prints was analyzed using a confocal microscope (microsurf custom microscope, NanoFocus, Oberhausen, Germany).

The electrical resistance of selected structures was determined using a parameter analyzer (Type HP4156a, Hewlett-Packard, Palo Alto, USA). The specific electrical resistance was calculated using the length of the printed structures and their cross section, which both had been determined by confocal microscopy.

#### Assembly of FETs

To study the electrical properties of the ITO inks, thin film transistors with a bottom gate, top-contact architecture were manufactured. The substrate was highly p-doped silicon with a 200-nm thermally grown silicon dioxide as gate insulator on the topside. The active layer was built with a dispersion of 10 wt% ZnO nano-particles in ethanol stabilized by TODA (VP ZnO 20, Evonik Industries AG, Germany). The dispersion was spun on the substrate and afterwards annealed at 400 °C under ambient atmosphere for 30 min in order to remove the TODA [19]. The source/drain electrodes were printed with the ITO-ink 2\_6.9 on the ZnO layer in ambient conditions. The dimensions of the electrodes were 2 × 0.5 mm<sup>2</sup> with a 50-μm space between them. A schematic drawing of the FET manufactured is shown in Fig. 2. The samples were cured in a furnace at 400 °C for 30 min to remove also the TODA of the ITO prints. The electrical characterization of the devices was conducted with a parameter analyzer (Type Keithley 2636, Cleveland, USA) under nitrogen atmosphere in order to reduce the influence of humidity and oxygen. To control the dimensions of the electrodes and the quality of the ZnO and the ITO layers the samples were analyzed by a SEM (Type JEOL, JSM-7500F, Tokyo, Japan). The cross section was prepared by breaking the sample after preparing a predetermined breaking point with a diamond tip.

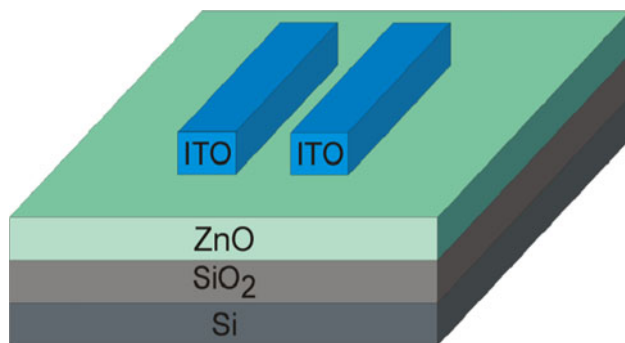


**Fig. 2** Schematic drawing of the FET assembled

## Results and discussion

### Characterization of dispersions

To study the influence of the different solvents on the inks' characteristics, the dispersions described with pure solvents and different solids loadings were prepared and characterized. For the preparation of inks, a solvent mixture was applied to adapt the properties of the inks to the inkjet process.

The mean particle size  $d_{50,vol}$  of dispersions in ethanol, ethylene glycol, and water with different solids loadings is depicted in Fig. 3. It can be clearly seen, that the agglomerate size in water and ethylene glycol remains almost constant and varies around 60–80 nm, whereas the agglomerate size in ethanol-based dispersions increases with increasing solids loading from 80 to 130 nm. Thus, the agglomerate size in the dispersions is in general very small, but the dispersion of the particles in water and ethylene glycol seems to be even more efficient. An increased tendency to agglomeration can be observed in ethanol-based dispersions with higher solids loadings.

On a microscopic scale, the observed effect might be explained by the differences in dielectric constant of the chosen solvents. TODA is an electrosteric dispersant, for which the DLVO-theory can often be applied [20]. According to DLVO calculations, the repulsive Coulomb force is increased with an increase in the dielectric constant of the dispersion media. This would be in good accordance with the experimental results, as ethanol exhibits a dielectric constant of 24, ethylene glycol of 38, and water of 80, respectively, and therefore the smallest repulsive forces can be expected for ethanol. Nevertheless, other publications reveal that this explanation might be too simple due to the complex adsorption behavior of TODA [21, 22].

The DLS measurements conducted are confirmed qualitatively by oscillatory rheological measurements. In Fig. 4 the loss angle of the dispersions in ethanol, ethylene glycol, and water with different solids contents is plotted. The loss angle was calculated for measuring values in the linear viscoelastic regime, therefore, it yields information about

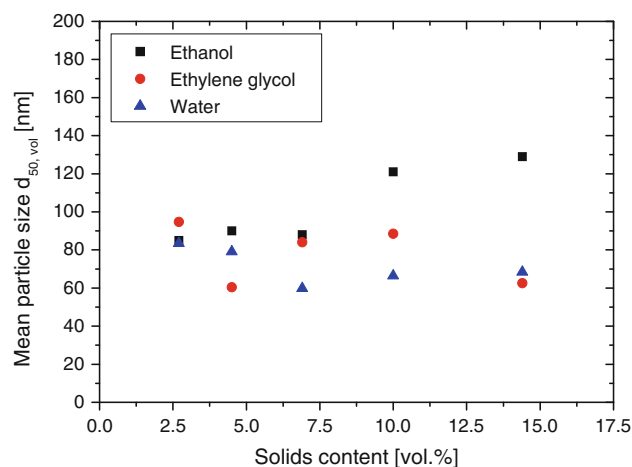


**Fig. 3** Mean particle size  $d_{50,vol}$  of ITO dispersions in ethanol, ethylene glycol, and water with different solids loadings

the structure of the dispersions at rest [23, 24]. The loss angle  $\delta$  is defined as follows:

$$\tan \delta = \frac{G''}{G'} \quad (4)$$

where  $G''$  is the loss modulus and  $G'$  is the storage modulus. A perfect solid would have a loss angle of  $0^\circ$  and a perfect liquid a loss angle of  $90^\circ$ , viscoelastic substances have values in between. The plot in Fig. 4 shows that all dispersions exhibit a loss angle of almost  $90^\circ$  up to a solids content of 3 vol. %. No particle–particle interaction can be recognized in the rheological measurements. For higher solids loadings, first the ethanol-based dispersions, then the ethylene glycol dispersions feature viscoelastic behavior. This means that the particle–particle interactions become increasingly important and the tendency of particles to agglomeration increases. This cannot be observed for any water-based dispersion measured; therefore, water is the most suitable dispersion media analyzed. The results are in good agreement with the DLS measurements.

The viscosity of the dispersions determined at a shear rate of  $200 \text{ s}^{-1}$  using rotational rheological measurements is depicted in Fig. 5. The viscosity of all dispersions generally increases with increasing particle content as expected. Dispersions based on ethylene glycol exhibit the highest viscosities because also the viscosity of the pure solvent ethylene glycol is the highest. The viscosity of pure ethylene glycol is 16.1 mPa s, whereas ethanol exhibits a viscosity of 1.1 mPa s and water a viscosity of 0.9 mPa s at  $25^\circ \text{C}$ . The steepest increase in viscosity with increasing solids loading can be seen for the ethanol-based dispersions due to their increased tendency to agglomeration at higher solids content as discussed before. To conclude, it can be observed that the dispersions in general exhibit low viscosities not exceeding 320 mPa s.

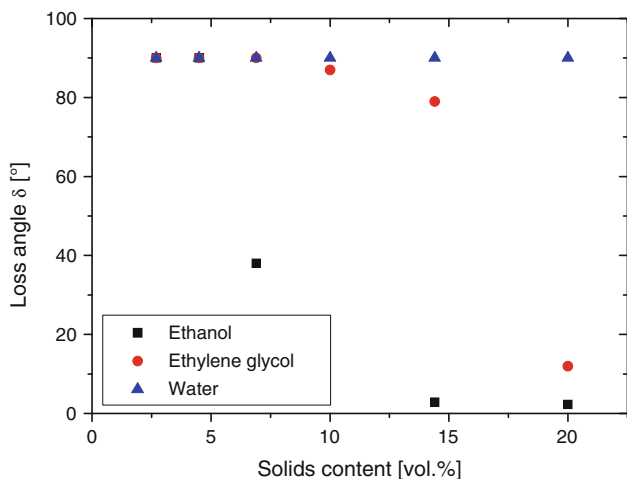


**Fig. 4** Loss angle of ITO dispersions in ethanol, ethylene glycol, and water with different solids loading determined using oscillatory rheological measurements; the loss angle was determined in the linear viscoelastic regime

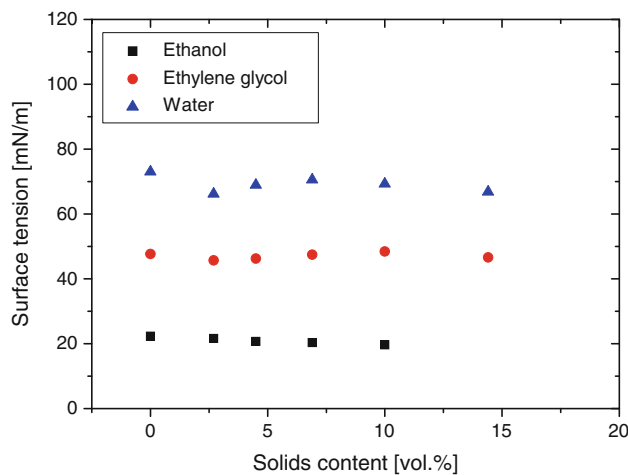


**Fig. 6** Surface tension of ITO dispersions in ethanol, ethylene glycol, and water with different solids loadings

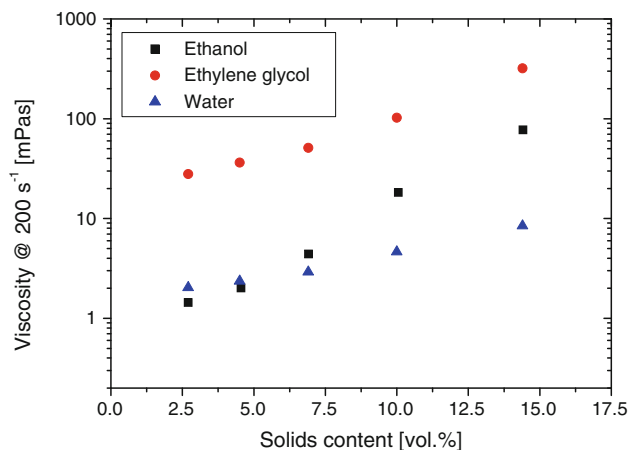


**Fig. 5** Viscosity at a shear rate of  $200\text{ s}^{-1}$  of ITO dispersions in ethanol, ethylene glycol, and water with different solids loadings

As the surface tension of inks has a significant influence on drop formation during inkjet printing as well as on the geometry of the printed structures, the surface tensions of the dispersions in ethanol, ethylene glycol, and water have also been characterized. The results are shown in Fig. 6. It can be seen that the surface tension of the dispersions exhibits nearly no dependency on the solids content in the dispersions. The surface tension of the dispersions are equal to the surface tension of the pure solvents, which is 22 mN/m for ethanol, 48 mN/m for ethylene glycol, and 72 mN/m for water.

**Characterization of inks**

In order to prepare inks for the inkjet printing process with adapted properties, dispersions in solvent mixtures have been prepared. In total, three solvent mixtures 1–3 were

**Table 2** Particle size and rheological properties of inks

Ink	$d_{50,vol}$ (nm)	Loss angle (°)	Viscosity @ $200\text{ s}^{-1}$ (mPa s)
Ink 1_6.9	35	90	14
Ink 2_2	59	90	11
Ink 2_6.9	56	90	25
Ink 2_9	69	90	35
Ink 3_6.9	59	90	27

**Table 3** Wetting behavior of inks

Ink	Surface tension (mN/m)	Contact angle on Si wafer (°)	Contact angle on PET (°)
Ink 1_6.9	30.4	32.4	61.0
Ink 2_2	34.1	30.5	65.2
Ink 2_6.9	34.9	30.3	59.4
Ink 2_9	32.4	35.0	62.8
Ink 3_6.9	32.5	– <sup>a</sup>	48.5

<sup>a</sup> Too low to be measured, immediate spreading

tested. To analyze the influence of the solids loading on the printing process and the printed structures, the ITO content was varied between 2 and 9 vol. % using solvent mixture 2.

The properties of the inks are summarized in Tables 2 and 3. The agglomerate size in dispersions measured using DLS is below 70 nm and thus the particles could be effectively dispersed in all solvent mixtures. This is confirmed by oscillatory rheological measurements: the loss angle of all dispersions is  $90^\circ$  thus no particle network

**Table 4** Z-Parameter of the inks prepared

Ink	Z-Parameter
Ink 1_6.9	2.14
Ink 2_2	2.63
Ink 2_6.9	1.29
Ink 2_9	0.93
Ink 3_6.9	1.15

formation can be monitored. Besides, also the viscosities are very low and all inks except Ink 2\_9 have a viscosity below 30 mPa s and meet the specifications of the printer applied [25]. Only Ink 2\_9 exhibits a value of 32 mPa s which is slightly above this value due to the increased solids loading compared to the other inks.

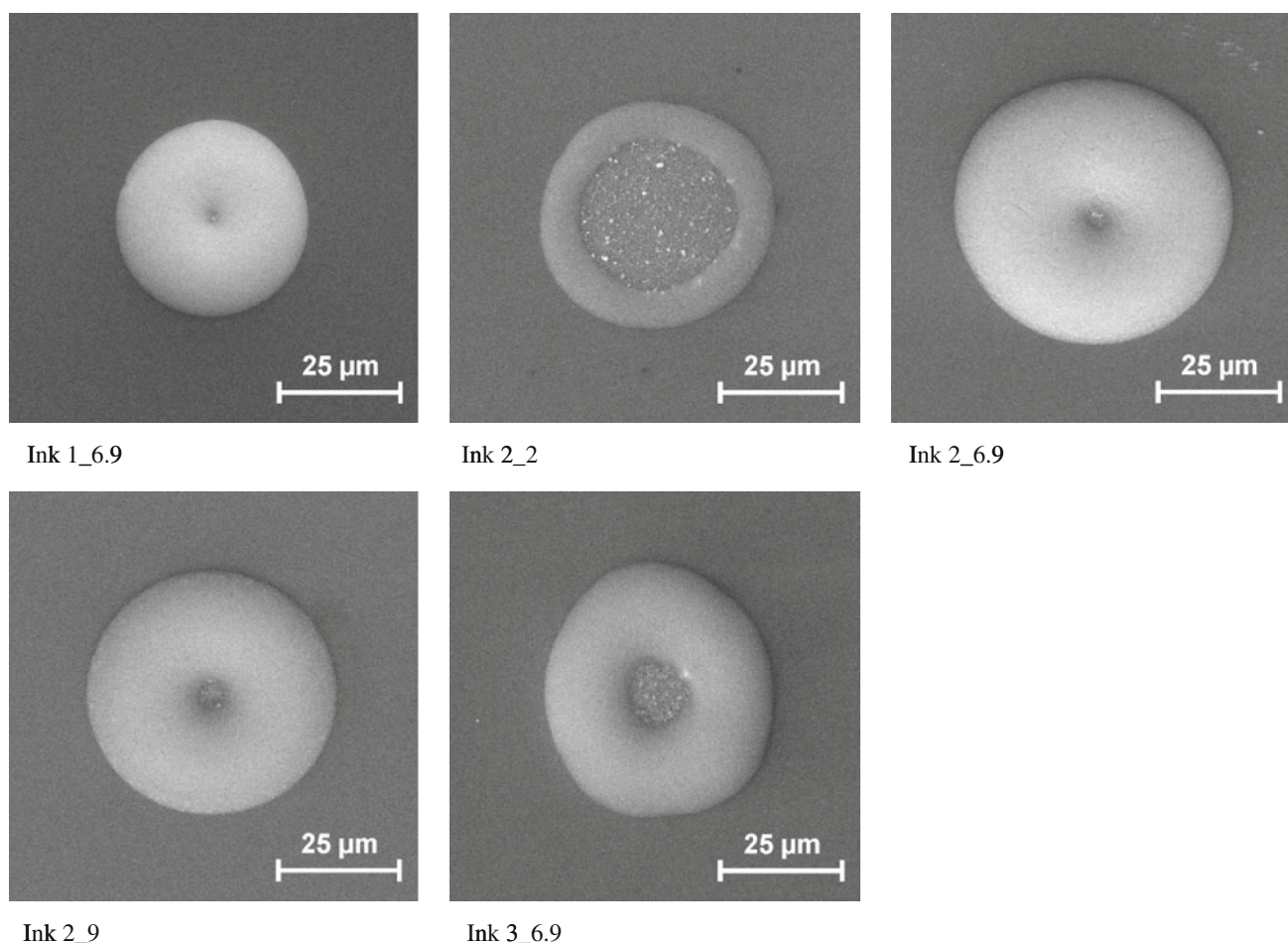
Furthermore, the wetting behavior of the inks is also displayed in Table 3. The surface tensions of all inks are very similar and comparably low in the range of 30–35 mN/m. Concerning the substrates used for printing, this results in low contact angles of up to 35° on silicon wafer and medium contact angles in the range of 45° to 65°

on PET sheets. The measured surface energy of the silicon wafer was 51.3 mN/m and thus higher than the surface energy of the PET tape with 35.9 mN/m.

To judge the printability of the inks, the Z-parameter has been calculated for all inks prepared according to Formula (3). The results are displayed in Table 4. It can be seen, that nearly all the inks are in the desired regime for Z values from 1 to 10, only ink 2\_9 is slightly below with a Z value of 0.93. In general, the Z values calculated range from 0.93 to 2.63 and thus are rather low. This can be explained by the fact, that the viscosity is the dominant parameter in Formula (3) because all other parameters only contribute with their square root. Viscosities of particulate inks at high solids loadings are generally higher than viscosities of precursor systems, therefore it is difficult to produce particulate inks with a high solids loading and a high Z value.

#### Printing of the inks

Like predicted by the Z value, all inks could be printed with the inkjet printer. Single drops on wafer are shown in SEM

**Fig. 7** SEM micrographs of drops of different ITO inks printed on wafer

**Table 5** Height and width of printed dots and thinnest printable lines on wafer and PET; if coffee-ring formation was observed, the height of the structures is defined as the maximum height of the prints

	Si wafer				PET			
	Dots		Lines		Dots		Lines	
	Height (μm)	Width (μm)	Height (μm)	Width (μm)	Height (μm)	Width (μm)	Height (μm)	Width (μm)
Ink 1_6.9	0.35	45	0.52	45	1.7	30	1.7	35
Ink 2_2	0.23	55	0.15 <sup>a</sup>	55 <sup>a</sup>	0.7	40	0.7	30
Ink 2_6.9	0.44	65	0.70 <sup>b</sup>	50 <sup>b</sup>	1.9	35	2.1	35
Ink 2_9	0.47	55	0.47 <sup>a</sup>	55 <sup>a</sup>	2.5	35	2.5	35
Ink 3_6.9	0.37	55	0.34 <sup>b</sup>	45 <sup>b</sup>	1.8	25	1.9	25

Drop spacing for the generation of lines is 20 μm, except: <sup>a</sup> drop spacing 30 μm, <sup>b</sup> drop spacing 40 μm

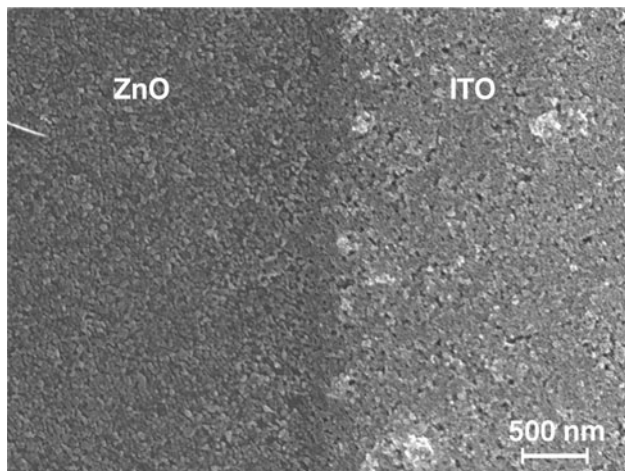


**Fig. 8** SEM micrograph of the interface between the ITO electrode and the ZnO semiconducting layer (vertical cross section of the electrode/semiconducting layer prepared by breaking the wafer)

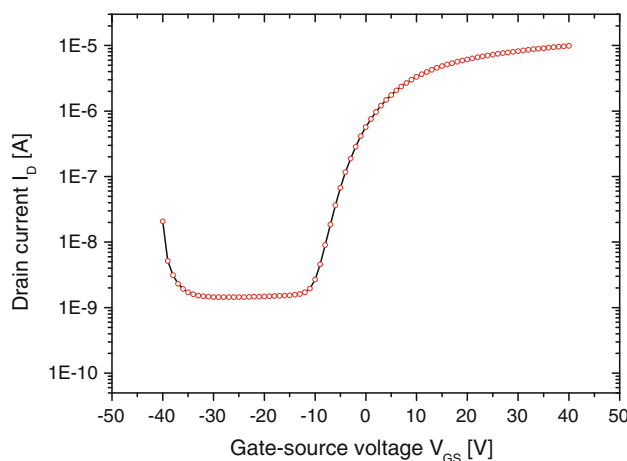


**Fig. 10** Transfer characteristic of the FET measured at a drain-source voltage of 10 V

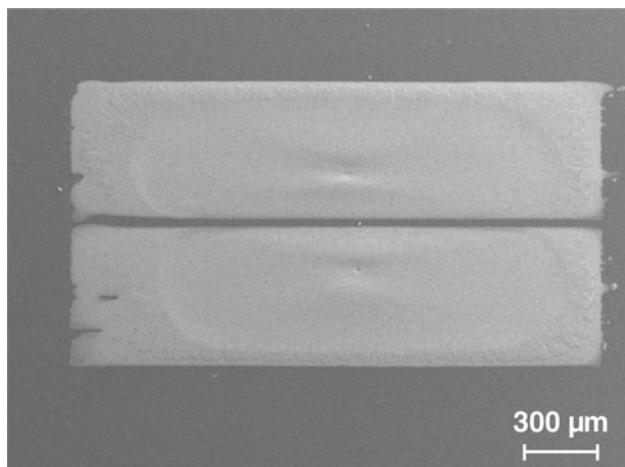


**Fig. 9** SEM top view of the printed ITO electrodes on ZnO layer,  $L = 35 \mu\text{m}$ ,  $W = 2040 \mu\text{m}$

micrographs in Fig. 7. A coffee-ring effect can be seen in all of the prints, i.e., the outer edge of the drops is higher compared to the middle due to particle migration from the middle to the edges during drying [26]. This effect is the most pronounced for Ink 2\_2 and Ink 3\_6.9. It is most likely, that in Ink 2\_2 the solids loading was too low. Only a minor coffee-ring can be observed for Ink 2\_6.9, which is based on the same solvent mixture but exhibits higher solids loading. The more pronounced coffee-ring effect of the printed drop of Ink 3\_6.9 can probably be assigned to the lower water content in this ink. Due to the almost perfect wetting of the ink on the wafer (see Table 3), the contact line of the drop is pinned and no receding of the ink on the wafer is possible.

Table 5 summarizes the dimensions of printed drops and lines on PET and wafer. The diameter of the drops nearly equals the diameter of the lines for each ink on the same substrate. In general, due to the higher contact angles,

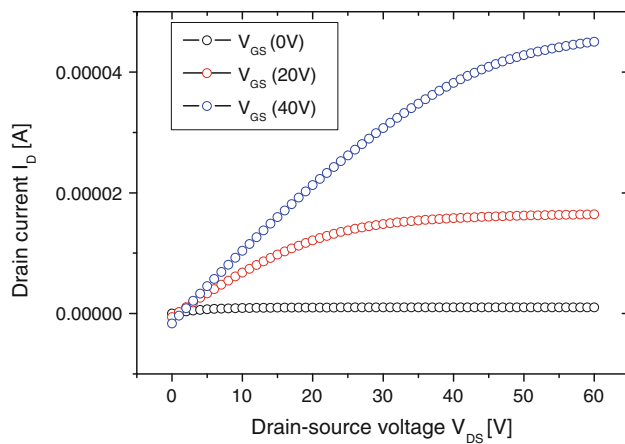


**Fig. 11** Output characteristic of the FET

thinner lines with a smaller width can be printed on PET, but also the crack formation is more pronounced on this substrate. Nevertheless, the prints exhibit a very good resolution with a minimum drop diameter of 30  $\mu\text{m}$  on PET and 45  $\mu\text{m}$  on wafer. Furthermore, investigations of the prints showed that the formation of the coffee-ring effect in the lines is analogous to the coffee-ring formation of the printed drops, i.e., the difference in height between the edges and the middle of the printed lines is the highest for Ink 2\_2 and Ink 3\_6.9.

For further printing experiments, the Ink 2\_6.9 was used as the most suitable of the inks prepared. It could be printed with the inkjet printer over a long time without major problems and line formation in horizontal and vertical direction was good. In contrast, the coffee-ring effect in printed structures of Inks 2\_2 and Ink 3\_6.9 is very strong as discussed above. Ink 1\_6.9 is not suitable because an “ink pillow” formed from time to time around the nozzle during printing, which then deflected the drops coming out of the nozzle. This had a negative effect on the structure formation. The reason for the formation of this “ink pillow” is not completely understood up to now. Most likely the contact angle of the ink on the printhead is very low leading to the wetting problems observed. Using Ink 2\_9, the nozzle was clogged from time to time. This effect can be assigned to the high particle loading in the ink and its tendency to form agglomerates.

#### Assembly of a FET

SEM micrographs of the ITO structures printed on ZnO can be seen in Figs. 8 and 9. The thickness of the ZnO layer is around 50 nm and the ITO electrodes show a maximum thickness of up to 4.7  $\mu\text{m}$ . The channel length  $L$  of the device is 35  $\mu\text{m}$  and the width  $W$  is 2040  $\mu\text{m}$ . The particles are densely packed but not sintered to a closed film. The space between the two ITO electrodes is constant

with the exception of the left edges, which is caused by bulging effects.

The transfer and output characteristics of this printed FET are shown in Figs. 10 and 11, respectively. The output characteristics display a linear slope for low drain-source voltages, indicating an ohmic contact between the ZnO film and the ITO contacts. The suitability of ITO source and drain contacts in ZnO FETs was already shown by Hoffman et al. [27]. By plotting the square root of the drain current ( $\sqrt{I_{\text{Dsat}}}$ ) versus the gate-source voltage ( $V_{\text{GS}}$ ) the charge carrier mobility ( $\mu_{\text{sat}}$ ) was calculated with a linear fit of the graph in the saturation region. The mobility was calculated according to Formula (5):

$$\mu_{\text{sat}} = \left( \frac{\partial \sqrt{I_{\text{Dsat}}}}{\partial V_{\text{GS}}} \right)^2 \cdot \frac{2L}{WC_{\text{is}}} \Bigg|_{V_{\text{DS}} > (V_{\text{GS}} - V_{\text{T}})} \quad (5)$$

$C_{\text{is}}$  the capacity of the gate insulator,  $V_{\text{DS}}$  the drain-source voltage, and  $V_{\text{T}}$  the threshold voltage. The carrier mobility is  $5 \times 10^{-3} \text{ cm}^2 (\text{V s})^{-1}$  and the  $I_{\text{on}}/I_{\text{off}}$  ratio is in the range of  $5 \times 10^3$ – $1.0 \times 10^5$  which is in good agreement with the values of Walther et al. [19] with the same ZnO material and evaporated aluminum contacts. In conclusion, the printed ITO electrodes are fully functional and can replace evaporated aluminum contacts in FETs leading to the same electrical performance of the electron device.

#### Conclusions

ITO inkjet inks could be successfully prepared and printed. For ink preparation it is of utmost importance to achieve full deagglomeration of the nano-sized powder and to adjust the rheological and wetting behavior of the inks. A minimum line width of 30  $\mu\text{m}$  on PET and 45  $\mu\text{m}$  on silicon wafer was achieved. The inks could also be printed on a nano-particulate ZnO layer to assemble a FET with the ITO prints as electrodes. The device showed similar transfer and output characteristics as a comparable device with evaporated aluminum contacts thus proving the electrical functionality of the FET.

**Acknowledgements** The financial support of the German Research Foundation (DFG, Graduiertenkolleg1161) as well as the support of our industrial partner Evonik Industries AG, Germany, is gratefully acknowledged.

#### References

1. Calvert P (2001) Chem Mater 13(10):3299
2. Hoffmann RC, Dilfer S, Schneider JJ (2011) Phys Status Solidi A 208:2920
3. Zhang XH, Lee SM, Domercq B, Kippelen B (2008) Appl Phys Lett 92:2433071



4. Le HP (1998) *J Imaging Sci Technol* 42(1):49
5. Lejeune M, Chartier T, C. Dossou-Yovo C, Noguera R (2009) *J Eur Ceram Soc* 29(5):905
6. Singh M, Haverinen HM, Dhagat P, Jabbour GE (2010) *Adv Mater* 22(6):673
7. Caironi M, Gili E, Sakanoue T, Cheng X, Sirringhaus H (2010) *ACS Nano* 4(3):1451
8. Hwang MS, Jeong BY, Moon J, Chun SK, Kim J (2011) *Mater Sci Eng, B* 176(14):1128
9. Fromm JE (1984) *IBM J Res Dev* 28(3):322
10. Derby B, Reis N (2003) *MRS Bull* 28(11):815
11. Jang D, Kim D, Moon J (2009) *Langmuir* 25(5):2629
12. Derby B (2010) *Annu Rev Mater Res* 40:395
13. Schiaffino S, Sonin AA (1997) *J Fluid Mech* 343:95
14. Duineveld PC (2003) *J Fluid Mech* 477:175
15. Stringer J, Derby B (2010) *Langmuir* 26(12):10365
16. Straue N, Rauscher M, Walther S, Faber H, Roosen A (2009) *J Mater Sci* 44(22):6011. doi:10.1007/s10853-009-3804-1
17. Reindl A, Mahajeri M, Hanft J, Peukert W (2009) *Thin Solid Film* 517:1624
18. Mahajeri M, Voigt M, Klupp Taylor RN, Reindl A, Peukert W (2010) *Thin Solid Films* 518:3373
19. Walther S, Schäfer S, Jank MPM, Thiem H, Peukert W, Frey L, Ryssel H (2010) *Microelectron Eng* 87(11):2312
20. Reindl A (2009) PhD thesis, Department of Chemical and Biological Engineering, University of Erlangen-Nuremberg
21. Renger C, Kuschel P, Kristoffersson A, Clauss B, Oppermann W, Sigmund W (2004) *Phys Chem Chem Phys* 6(7):1467
22. Finke T, Lingenfeller D, Bindler K, Eisele U, Bockhorn H, Brunklaus G (2009) *J Am Ceram Soc* 92(8):1823
23. Bergström L (1994) In: Pugh R (ed) Bergström L (ed), Dekker M (ed) *Surfactant science series*, vol 51. Surfactant and colloid chemistry in advanced ceramics processing, New York
24. Renger C, Kuschel P, Kristoffersson A, Clauss B, Oppermann W, Sigmund W (2007) *J Eur Ceram Soc* 27(6):2361
25. Printer FAQs-Dimatix (2011) FUJIFILM Dimatix Inc., Santa Clara, CA, USA. [http://www.dimatix.com/files/printer\\_faqs.pdf](http://www.dimatix.com/files/printer_faqs.pdf). Accessed 01 June 2011
26. Deegan RD, Bakajin O, Dupont TF, Huber G, Nagel SR, Witten TA (1997) *Nature* 389:827
27. Hoffman RL, Norris BJ, Wager JF (2003) *Appl Phys Lett* 82:733